Object-oriented electrodynamic transfer matrix code with modern applications[☆]

Alex J. Yuffa[*], John A. Scales

Department of Physics, Colorado School of Mines, Golden, Colorado 80401, USA

Abstract

The transfer matrix algorithm for the propagation of an electromagnetic wave through planar stratified media has been implemented in a modern objected-oriented programming language. The implementation is suitable for the study of applications such as the Anderson localization of light and super-resolution (perfect lensing). For our open-source code to be as useful as possible to the scientific community, we paid particular attention to the pathological cases that arise in the limit of vanishing absorption.

Keywords: Wave propagation, Electromagnetic scattering, Transfer matrix method, Negative refractive material
PACS: [2010] 01.50.hv, 42.25.Bs, 42.25.Dd, 42.25.Fx, 42.25.Gy

Program summary

Manuscript Title: Object-oriented electrodynamic transfer matrix code with modern applications
Authors: Alex J. Yuffa, John A. Scales
Program Title: openTMM
Journal Reference:
Catalogue identifier:
Licensing provisions: The MIT License
Programming language: Python, Fortran 90
Computer: x86
Operating system: Linux, Unix, MacOS X, Windows
RAM: 10 MB
Keywords: Wave propagation, Electromagnetic scattering, Transfer matrix method, Negative refractive material.
Classification: 10
External libraries: SciPy (`http://www.scipy.org/`)
Nature of problem: Electromagnetic wave propagation through planar stratified media (multilayer stack); the three-dimensional space is divided into layers. The interfaces separating the layers are assumed to be perfectly planar and the layers are assumed to be isotropic and homogeneous, with a complex permittivity and permeability. Moreover, the layers may be composed of a left-handed material (negative refractive material) and/or a right-handed material. The implementation is suitable for the study of modern applications, e.g., Anderson localization of light and sub-wavelength imaging.
Solution method: The transfer matrix method, with careful treatment of the pathological cases that arise in the limit of vanishing absorption.
Restrictions: If single precision accuracy is required, then the absorption of each layer should be small. Roughly speaking, the imaginary part of the wavenumber multiplied by the thickness of the layer should be on the order of one.
Unusual features: The layers may be composed of a left-handed and/or right-handed material with or without absorption.
Running time: Seconds to minutes

1. Introduction

Electromagnetic wave propagation through planar stratified media (multilayer stack) is a century old problem in physics. It may be somewhat surprising that it is still relevant today. In fact, it has only relatively recently discovered that the transmission and reflection coefficients for a multilayer stack may be written down without any computations by utilizing a complex version of the elementary symmetric functions [1, 2]. It has been also recently discovered that the complex reflection coefficients follow the generalized version of the composition law used to add parallel velocities in the theory of special relativity, see [3, 4] and Refs. within. Although it is possible to use the above mentioned properties to formulate a numerical wave propagation algorithm in planar stratified media, we follow a more traditional approach of the late 1940's, namely, the transfer matrix algorithm [5, 6, 7, 8]. Before considering the details of the transfer matrix algorithm and the need for its open

[☆]This paper and its associated computer program are available via the Computer Physics Communications homepage on ScienceDirect (`http://www.sciencedirect.com/science/journal/00104655`). The computer program is also available from `http://pypi.python.org/pypi/openTMM`.

[*]Corresponding author.
Email address: `ayuffa@gmail.com` (Alex J. Yuffa)
URL: `http://mesoscopic.mines.edu` (John A. Scales)

source implementation in a modern object oriented language, we briefly mention some of the current applications we had in mind when we wrote the code.

In 1968, Veselago [9] considered a hypothetical non-active material in which the real parts of the permittivity and permeability are simultaneously negative; we refer to such a material as a *left-handed material* (LHM), but it is also known as a *negative refractive material*. It was only in the early 2000's that such a material was artificially fabricated [10, 11] and this led to an explosion of papers on the LHM, see [12] and Refs. within. One of the intriguing proprieties of the LHM is the ability to image with a sub-wavelength image resolution (super-resolution if you will), which has been proposed and studied in the context of a multilayer stack. [13, 14] Another general area of application is the Anderson localization of light [15, 16], which has been studied both theoretically and experimentally by Scales et al. [17], who considered wave propagation at normal incidence through a multilayer stack made of quartz and Teflon wafers. The effects of total internal reflection on light localization in a random multilayer stack at oblique incidence have also been studied under the assumption of complete phase randomization [18] as well as the effects of the LHM on localization [19]. Other applications include the study of asymmetrical properties of light in a Fabry-Pérot interferometer [20, 21].

In all of the above applications, the transfer matrix algorithm was or could have been used; however, to the best of our knowledge, an open-source and object-oriented implementation of the transfer matrix algorithm suitable for the LHM as well as the right-handed material (RHM) (where the real parts of the permittivity and permeability are *not* simultaneously negative) is currently unavailable. Without a doubt there are many "in-house" implementations of the transfer matrix algorithm, but in the context of reproducibility of scientific work, it is important to have an open-source and publicly available implementation. Moreover, as it will be discussed later, there are some pathological cases where the numerical implementation is not clear. This paper is self-contained as much as possible in order for our implementation of the transfer matrix algorithm to be as useful as possible to the widest possible scientific community. We also point out the benefits and drawbacks of using a high-level programming language called Python[1] for implementing our code, see Section 8.

2. Background

The source-free macroscopic Maxwell equations with assumed harmonic time dependence, $\exp(-i\omega t)$, in the Système International (SI) unit system, at every ordinary point in space, are:

$$\nabla \cdot \mathbf{D} = 0, \qquad \nabla \cdot \mathbf{B} = 0, \tag{1a}$$

$$\nabla \times \mathbf{E} = i\omega \mathbf{B}, \qquad \nabla \times \mathbf{H} = -i\omega \mathbf{D}, \tag{1b}$$

where $\mathbf{E}$ is the electric field, $\mathbf{D}$ is the displacement field, $\mathbf{B}$ is the magnetic field, $\mathbf{H}$ is the magnetic intensity, and ω is the angular frequency. By an ordinary point in space, we mean a point in space in whose "neighborhood" the physical properties of the medium are continuous. Thus, strictly speaking, one cannot apply Maxwell's equations at a surface that separates two physically different media. If the medium is isotropic and homogeneous, then $\mathbf{D} = \epsilon \mathbf{E}$ and $\mathbf{B} = \mu \mathbf{H}$, where ϵ and μ are the permittivity and the permeability, respectively. Permittivity must satisfy the Kramers-Kronig relations and is therefore a complex-valued function of angular frequency. The same is true for permeability. Thus, in general, we have $\epsilon = \epsilon(\omega) \in \mathbb{C}$ and $\mu = \mu(\omega) \in \mathbb{C}$.

The source-free macroscopic Maxwell equations are first-order linear partial differential equations (PDEs) that must be supplemented by some boundary conditions. The conventional boundary conditions for a source-free interface separating two media (1 and 2) are:

$$\mathbf{n} \cdot \left(\mathbf{D}^{(2)} - \mathbf{D}^{(1)}\right) = 0, \qquad \mathbf{n} \cdot \left(\mathbf{B}^{(2)} - \mathbf{B}^{(1)}\right) = 0, \tag{2a}$$

$$\mathbf{n} \times \left(\mathbf{E}^{(2)} - \mathbf{E}^{(1)}\right) = \mathbf{0}, \qquad \mathbf{n} \times \left(\mathbf{H}^{(2)} - \mathbf{H}^{(1)}\right) = \mathbf{0}, \tag{2b}$$

where $\mathbf{n}$ is a unit normal to the interface, and the superscript on the fields indicates from which medium the interface is approached.

Taking the curl of (1b), then simplifying the result using the $\nabla \times (\nabla \times \mathbf{A}) = \nabla(\nabla \cdot \mathbf{A}) - \nabla^2 \mathbf{A}$ vector identity and (1a), we obtain the vector Helmholtz equation within each layer

$$\left(\nabla^2 + k^2\right) \begin{Bmatrix} \mathbf{E} \\ \mathbf{H} \end{Bmatrix} = \mathbf{0}, \tag{3}$$

where k is the complex wavenumber, and $k^2 = \mu\epsilon\omega^2$. In general, $k^2 \neq kk^*$, where * denotes the complex conjugate, and the computation of k from k^2 must be done with extreme care. For example, permittivity and permeability for an absorbing material are taken to be $\epsilon = \epsilon' + i\epsilon''$ and $\mu = \mu' + i\mu''$, respectively, where $\{\epsilon', \mu', \} \in \mathbb{R}, \{\epsilon'', \mu''\} \in \mathbb{R}^+$.[2] Let $\epsilon = |\epsilon| e^{i\theta_\epsilon}$ and

[1] Python is free and open-source software that runs on Windows, Linux/Unix, Mac OS X, Java and .NET virtual machines. It may be downloaded from http://www.python.org/.

[2] For the $\exp(+i\omega t)$ time dependence, $\epsilon = \epsilon' - i\epsilon''$, $\mu = \mu' - i\mu''$, where $\{\epsilon', \mu', \} \in \mathbb{R}, \{\epsilon'', \mu''\} \in \mathbb{R}^+$.

$\mu = |\mu|e^{i\theta_\mu}$, where $\{\theta_\epsilon, \theta_\mu\} \in [0, \pi]$.[3] Then

$$\begin{aligned} k^2 &= \epsilon\mu\omega^2 \\ k &= \sqrt{|\epsilon||\mu|}\omega e^{i\left(\frac{\theta_\epsilon+\theta_\mu+2\pi n}{2}\right)}, \qquad n = 0, 1, \\ &= \sqrt{|\epsilon||\mu|}\omega \left\{ e^{i\left(\frac{\theta_\epsilon+\theta_\mu}{2}\right)}, e^{i\left(\frac{\theta_\epsilon+\theta_\mu}{2}+\pi\right)} \right\}, \end{aligned} \tag{4}$$

where $\omega > 0$. The choice of the root in (4) is dictated by the physical requirement that in an absorbing medium the wave must decay and not exponentially grow. Let $k = k' + ik''$, $\{k', k''\} \in \mathbb{R}$. Without loss of generality, consider a plane wave propagating in the *positive* x-direction; then, we have $e^{i(kx-\omega t)} = e^{-k''x}e^{i(k'x-\omega t)}$. Therefore, k'' must be *greater than zero* in order for the wave to decay in the positive x-direction.

2.1. Pathological cases at normal incidence

In the case of a perfect dielectric ($\epsilon'' = 0$ and $\mu'' = 0$), the rule for choosing a physically appropriate root in (4) may be established by taking a limit as absorption goes to zero.

Consider an almost perfect dielectric made of the RHM. Let $\epsilon = |\epsilon|e^{i\theta_\epsilon}$, $\mu = |\mu|e^{i\theta_\mu}$, where θ_ϵ and θ_μ are infinitesimally small *positive* numbers, then $\frac{\theta_\epsilon+\theta_\mu}{2} \ll \pi$ and $\frac{\theta_\epsilon+\theta_\mu}{2} + \pi > \pi$. Thus, we must choose the first root in (4), i.e., $k = \sqrt{|\epsilon||\mu|}e^{i\left(\frac{\theta_\epsilon+\theta_\mu}{2}\right)}\omega$. In the case of a truly perfect dielectric (at fixed frequency), we may take the limit as θ_ϵ and θ_μ approach zero to obtain $k = \sqrt{|\epsilon||\mu|}\omega$.

In the case of an almost perfect dielectric made of a LHM: Let $\epsilon = |\epsilon|e^{i\theta_\epsilon}$, $\mu = |\mu|e^{i\theta_\mu}$, where θ_ϵ and θ_μ are slightly *less than* π, then $\frac{\theta_\epsilon+\theta_\mu}{2} < \pi$ and $\frac{\theta_\epsilon+\theta_\mu}{2} + \pi > \pi$. Thus, we must choose the first root in (4), i.e., $k = \sqrt{|\epsilon||\mu|}e^{i\left(\frac{\theta_\epsilon+\theta_\mu}{2}\right)}\omega$. For a truly perfect dielectric (at fixed frequency), we may take the limit as θ_ϵ and θ_μ approach π to obtain $k = \sqrt{|\epsilon||\mu|}e^{i\pi}\omega = -\sqrt{|\epsilon||\mu|}\omega$. Notice that for the LHM with zero absorption, $k < 0$, and for the RHM with zero absorption, $k > 0$.

3. Wave propagation in stratified media

Consider the three-dimensional space divided into $p + 1$ regions. The regions are infinite in the yz-plane, see Figure 1. The interfaces separating the regions are assumed to be perfectly planar (yz-plane). The regions $\ell = 0, \ldots, p-1$ are assumed to be isotropic and homogeneous with a complex permittivity, ϵ_ℓ, and complex permeability, μ_ℓ, where ℓ denotes the region number as shown in Figure 1. The p^{th} region is assumed to be isotropic and homogeneous with real permittivity, ϵ_p, and real permeability, μ_p. In other words, we have $\{\epsilon_\ell, \mu_\ell\} \in \mathbb{C}$ for $\ell = 0, \ldots, p-1$ and $\{\epsilon_p, \mu_p\} \in \mathbb{R}$.

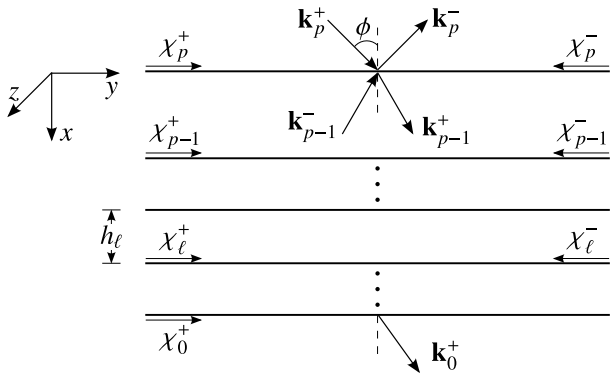

Figure 1: The cross-sectional view of the multilayer stack is shown. The multilayer stack consists of $p + 1$ regions made of a RHM. A parallel-polarized wave is incident from the p^{th} region. The origin of the coordinate system is set on the planar interface separating regions p and $p - 1$.

A monochromatic plane wave in ℓ^{th} region is given by

$$\begin{Bmatrix} \mathbf{E}_\ell(\mathbf{r}, t) \\ \mathbf{H}_\ell(\mathbf{r}, t) \end{Bmatrix} = \begin{Bmatrix} \mathbf{E}_\ell \\ \mathbf{H}_\ell \end{Bmatrix} e^{i(\mathbf{k}_\ell \cdot \mathbf{r} - \omega t)}, \tag{5}$$

where $\mathbf{r} = x\,\hat{\mathbf{x}} + y\,\hat{\mathbf{y}} + z\,\hat{\mathbf{z}}$, $\{\mathbf{E}_\ell, \mathbf{H}_\ell\}$ are the *complex* vector amplitudes, $\mathbf{k}_\ell = k_{x,\ell}\,\hat{\mathbf{x}} + k_{y,\ell}\,\hat{\mathbf{y}} + k_{z,\ell}\,\hat{\mathbf{z}}$ is the *complex* wavevector, and the subscript ℓ denotes the region label. In order to keep the formulas concise, the integer denoted by ℓ is assumed to take values $0, \ldots, p$ unless explicitly noted otherwise. It's clear that (5) satisfies (3) if

$$\mathbf{k}_\ell \cdot \mathbf{k}_\ell = k_{x,\ell}^2 + k_{y,\ell}^2 + k_{z,\ell}^2 = k_\ell^2 = \epsilon_l\mu_l\omega^2. \tag{6}$$

Without loss of generality, we can set $k_{z,\ell} = 0$ because we can always rotate the coordinate system so that the y-axis is parallel to the part of the $\mathbf{k}$ vector that lies in the yz-plane, see Figure 1.[4] The solution in each region given by (5) must also satisfy the boundary conditions given by (2).[5] From Snell's law, which can be derived from (2), we obtain

$$k_{y,p} = k_{y,\ell}, \qquad \ell = 0, \ldots, p-1, \tag{7}$$

where $k_{y,p} \in \mathbb{R}$ because we have tactfully assumed that the p^{th} region has real permittivity and permeability (see above).

[3] We always mean the *positive* square root of x when we write $\sqrt{x}$, where $x \in \mathbb{R}^+$. The fundamental issue with the $w = z^{\frac{1}{2}}$ mapping is that the "square root" function has *branch points* at $z = 0$ and $z = \infty$ and thus must have a *branch cut* connecting the two branch points, see [22, Vol. 1, Sec. 54].

[4] We could have chosen to set $k_{y,\ell} = 0$, and then rotated the coordinate system so that the z-axis is parallel to the part of the $\mathbf{k}$ vector that lies in the yz-plane. The main point is that $\mathbf{k}$ can always be made into a two-dimensional vector.

[5] It turns out that satisfying the boundary conditions and solving the wave equation is *not* enough to guarantee that the solution will also satisfy Maxwell's equations. These so-called "spurious" solutions have plagued finite-difference time-domain (FDTD) methods for some time now.[Sec. 2.10.5 23, 24, 25] We don't have to worry about such complications; our solution *does* satisfy Maxwell's equations.

Therefore, from (7) we have $k_{y,\ell} \in \mathbb{R}$, but note that in general, $k_{x,\ell} \in \mathbb{C}$ for $\ell = 0, \ldots, p-1$. Using (6) and (7) yields

$$k_{x,\ell} = \left(\epsilon_\ell \mu_\ell \omega^2 - k_{y,p}^2\right)^{1/2} \quad \text{with} \quad \mathrm{Im}[k_{x,\ell}] > 0, \tag{8}$$

where Im denotes the imaginary part and the root choice, $\mathrm{Im}[k_{x,\ell}] > 0$, is dictated by the decaying wave requirement, see Section 2.

3.1. Pathological cases at oblique incidence

It is clear from (8) that if $\epsilon_\ell'' = 0$, $\mu_\ell'' = 0$ and $\epsilon_\ell \mu_\ell \omega^2 > k_{y,p}^2$, then the root choice is not resolved by the $\mathrm{Im}[k_{x,\ell}] > 0$ requirement. In order to resolve the root choice, we proceed by taking a limit as absorption goes to zero just as we did in Section 2.1. For the RHM, let $\epsilon_\ell = |\epsilon_\ell| e^{i\theta_{\epsilon_\ell}}$, $\mu_\ell = |\mu_\ell| e^{i\theta_{\mu_\ell}}$ and for the LHM, let $\epsilon_\ell = |\epsilon_\ell| e^{i(\pi - \theta_{\epsilon_\ell})}$, $\mu_\ell = |\mu_\ell| e^{i(\pi - \theta_{\mu_\ell})}$, where θ_{ϵ_ℓ} and θ_{μ_ℓ} are infinitesimally small *positive* numbers. Then $k_{x,\ell}^2$ can be approximately written as $k_{x,\ell}^2 \approx |A| e^{\pm i\gamma}$, where $0 \le \gamma \ll \pi$, $\lim_{\{\epsilon_\ell'', \mu_\ell''\} \to 0} \gamma = 0$, and the positive (negative) sign in the exponential corresponds to the RHM (LHM). Thus, we have

$$\mathrm{Im}\left[k_{x,\ell}\right] = \sqrt{|A|}\left\{\pm \sin\left(\frac{\gamma}{2}\right), \pm \sin\left(\frac{\gamma}{2} + \pi\right)\right\}, \tag{9}$$

where it is clear that for the RHM (LHM) the first (second) root must be chosen in order for $\mathrm{Im}\left[k_{x,\ell}\right] > 0$. Therefore, if $\epsilon_\ell'' = 0$, $\mu_\ell'' = 0$ and $\epsilon_\ell \mu_\ell \omega^2 > k_{y,p}^2$, then for the RHM we have $k_{x,\ell} = +\sqrt{|\epsilon_\ell|\,|\mu_\ell|\,\omega^2 - k_{y,p}^2}$, and for the LHM we have $k_{x,\ell} = -\sqrt{|\epsilon_\ell|\,|\mu_\ell|\,\omega^2 - k_{y,p}^2}$.

3.2. Origin and numerical treatment of the pathologies

The limiting procedure carried out in Section 2.1 and 3.1 appears to be reasonable, but unfortunately, it's also not physically attainable, even in principle! If we view $\epsilon(\omega)$ and $\mu(\omega)$, where $\omega = \omega' + i\omega''$, in the context of the Kramers-Kronig relations, then $\epsilon(\omega)$ and $\mu(\omega)$ are analytic functions in the upper-half ω-plane. Furthermore, it can be shown that $\epsilon(\omega)$ and $\mu(\omega)$ are never purely real for any finite ω except for $\omega' = 0$ (positive imaginary axis), e.g., see [26, Section 123] and [27, Section 82]. Therefore, the common practice of replacing $\epsilon' + i\epsilon''$ by ϵ' and $\mu' + i\mu''$ by μ' even in an infinitesimally small ω' interval *cannot* be justified. Moreover, by considering the *global* behavior of $k_{x,\ell}$ it can be shown that for a non-active medium $k_{x,\ell}$ is never zero.[28] However, we see from (8) that $k_{x,\ell}$, for any $\ell \neq p$ may be equal to zero if ϵ_ℓ and μ_ℓ are purely real. Of course, this case only occurs when the angle of incidence precisely equals one of the critical angles, and from the global properties of ϵ and μ we see that such angles *cannot* exists.

The above discussion suggests that the pathological cases only occur in an *unphysical* approximation, i.e., $\epsilon \approx \epsilon'$ and $\mu \approx \mu'$. In our numerical code, the user may select how to deal with the pathologies from the following two schemes:

1. If a region contains purely real permittivity and permeability, then the real permittivity and permeability are replaced by a slightly absorbing permittivity and permeability, respectively, i.e., for $\ell \neq p$, $\epsilon_\ell' \to \epsilon_\ell' + i\epsilon_\ell''$ and $\mu_\ell' \to \mu_\ell' + i\mu_\ell''$, where ϵ_ℓ'' and μ_ℓ'' are small positive numbers.
2. If a region contains purely real permittivity and permeability, then the $k_{x,\ell}$ is computed as describe in Section 2.1 and 3.1. If this scheme is chosen, then the code may produce erroneous results at or very near the critical angles.

3.3. Polarization

The most general polarization state is an *elliptical* polarization state. However, there is no need to consider this general case because an elliptical polarization state can always be decomposed into a linear combination of two linearly independent polarization states, namely, the *parallel* polarization state and the *perpendicular* polarization state. In what follows, it is convenient to express $\mathbf{E}_\ell(\mathbf{r}, t)$ and $\mathbf{H}_\ell(\mathbf{r}, t)$ in terms of each other by substituting (5) into (1b) (with $\mathbf{D}_\ell = \epsilon_\ell \mathbf{E}_\ell$) and using the vector identity

$$\nabla \times \begin{Bmatrix} \mathbf{E}_\ell(\mathbf{r}, t) \\ \mathbf{H}_\ell(\mathbf{r}, t) \end{Bmatrix} = i\mathbf{k}_\ell \times \begin{Bmatrix} \mathbf{E}_\ell \\ \mathbf{H}_\ell \end{Bmatrix} e^{i(\mathbf{k}_\ell \cdot \mathbf{r} - \omega t)},$$

to obtain

$$\mathbf{E}_\ell(\mathbf{r}, t) = -\frac{\mathbf{k}_\ell \times \mathbf{H}_\ell(\mathbf{r}, t)}{\epsilon_\ell \omega}, \tag{10a}$$

$$\mathbf{H}_\ell(\mathbf{r}, t) = \frac{\mathbf{k}_\ell \times \mathbf{E}_\ell(\mathbf{r}, t)}{\mu_\ell \omega}. \tag{10b}$$

3.3.1. Parallel polarization

A monochromatic light is said to have parallel polarization if the electric field is parallel to the *plane of incidence*. The plane of incidence is defined by the wavevector $\mathbf{k}$ and the normal vector to the surface $\mathbf{n}$; i.e., $\mathbf{k}$ and $\mathbf{n}$ lie in the plane of incidence. From Figure 1, we have $\mathbf{k}$ in xy-plane and $\mathbf{n} = \pm\hat{\mathbf{x}}$, thus, the plane of incidence is the xy-plane.

Consider a parallel polarized incident plane wave of angular frequency ω propagating in the *positive* x-direction. Maxwell's equations (1) are first-order linear PDEs, thus, the total wave inside regions $\ell = 1, \ldots, p$ may be decomposed into reflected and transmitted waves with the following wavevectors:

$$\mathbf{k}_\ell^{\pm} = \pm k_{x,\ell}\,\hat{\mathbf{x}} + k_{y,\ell}\,\hat{\mathbf{y}} \tag{11}$$

where $k_{x,\ell}$ is given by (8), $k_{y,\ell}$ is given by (7), $^+$ indicates a transmitted wave propagating in the $+x$-direction, and $^-$ indicates a reflected wave propagating in the $-x$-direction;[6] notice

[6] To obtain $\mathbf{k}_\ell^-$ from $\mathbf{k}_\ell^+$ we have used the *law of reflection*, which can be derived from (2).

that there is no reflected wave in the 0^{th} region. The magnetic intensity in each region is given by

$$\mathbf{H}_\ell^\pm(\mathbf{r},t) = \epsilon_\ell \omega E_\ell^\pm \exp\left[\mathrm{i}\left(\mathbf{k}_\ell^\pm \cdot \mathbf{r} - \omega t\right)\right] \hat{\mathbf{z}}, \tag{12}$$

where E_ℓ^+ is the *complex* amplitude associated with the transmitted wave, E_ℓ^- is the *complex* amplitude associated with the reflected wave, and $E_{\ell=0}^- \equiv 0$. Substituting (12) into (10a) yields

$$\mathbf{E}_\ell^\pm(\mathbf{r},t) = E_\ell^\pm \exp\left[\mathrm{i}\left(\mathbf{k}_\ell^\pm \cdot \mathbf{r} - \omega t\right)\right]\left[-k_{y,\ell}\,\hat{\mathbf{x}} \pm k_{x,\ell}\,\hat{\mathbf{y}}\right]. \tag{13}$$

From (2b), we see that the parallel components of the total electric field and the total magnetic intensity are continuous across the interface. It is convenient to define a new symbol for the y-component of the electric field because the electric field has components both parallel and perpendicular to the interface. Let

$$\chi_\ell^\pm = \pm k_{x,\ell} E_\ell^\pm \exp\left[\pm \mathrm{i} k_{x,\ell} \sum_{s=\ell}^{p} h_s\right], \tag{14}$$

where h_ℓ is the thickness of the ℓ^{th} region and, for convenience, we set $h_{\ell=0} = h_{\ell=p} \equiv 0$. In (14), $\chi_\ell^\pm$, $\ell = 1,\ldots,p$, denotes the y-component of the electric field at the interface between regions ℓ and $\ell-1$ (the interface is approached from the ℓ^{th} region), and χ_0^+ denotes the y-component of the electric field at the interface between region 1 and 0 (the interface is approached from the 0^{th} region), see Figure 1. Expressing (12) in terms of (14) yields

$$\psi_\ell^\pm = \pm w_\ell \chi_\ell^\pm, \tag{15}$$

where

$$w_\ell = \frac{\epsilon_\ell \omega}{k_{x,\ell}}. \tag{16}$$

Finally, substituting (13) and (12) into (2b), and using (14) and (15) to simplify the result, yields

$$\begin{aligned} \chi_{\ell+1}^+ + \chi_{\ell+1}^- &= \mathrm{e}^{-\mathrm{i}k_{x,\ell}h_\ell}\chi_\ell^+ + \mathrm{e}^{+\mathrm{i}k_{x,\ell}h_\ell}\chi_\ell^-, \\ w_{\ell+1}\chi_{\ell+1}^+ - w_{\ell+1}\chi_{\ell+1}^- &= w_\ell \mathrm{e}^{-\mathrm{i}k_{x,\ell}h_\ell}\chi_\ell^+ - w_\ell \mathrm{e}^{+\mathrm{i}k_{x,\ell}h_\ell}\chi_\ell^-, \end{aligned} \tag{17}$$

for $\ell = 0,\ldots,p-1$. After we obtain a linear system for the perpendicular polarization case, we will solve the linear system given by (17), see Section 4.

3.3.2. *Perpendicular polarization*

A monochromatic light is said to have perpendicular polarization if the electric field is perpendicular to the *plane of incidence*. The electric field in each region is given by

$$\mathbf{E}_\ell^\pm(\mathbf{r},t) = E_\ell^\pm \exp\left[\mathrm{i}\left(\mathbf{k}_\ell^\pm \cdot \mathbf{r} - \omega t\right)\right] \hat{\mathbf{z}} \tag{18}$$

where $\mathbf{k}_\ell^\pm$ is given by (11), and the $^\pm$ superscripts have the same meaning as in Section 3.3.1. Also as in Section 3.3.1, we set $E_{\ell=0}^- \equiv 0$ because there is no reflected wave in the 0^{th} region. Substituting (18) into (10b) yields

$$\mathbf{H}_\ell^\pm(\mathbf{r},t) = \frac{E_\ell^\pm}{\mu_\ell \omega} \exp\left[\mathrm{i}\left(\mathbf{k}_\ell^\pm \cdot \mathbf{r} - \omega t\right)\right]\left[k_{y,\ell}\,\hat{\mathbf{x}} \mp k_{x,\ell}\,\hat{\mathbf{y}}\right]. \tag{19}$$

From (2b), we see that both the parallel component of the total electric field and the magnetic intensity are continuous across the interface. It is convenient to define a new symbol[7] for the z-component of the electric field. Let

$$\chi_\ell^\pm = E_\ell^\pm \exp\left[\pm \mathrm{i} k_{x,\ell} \sum_{s=\ell}^{p} h_s\right], \tag{20}$$

where h_ℓ is the same as in Section 3.3.1, $\chi_\ell^\pm$, where $\ell = 1,\ldots,p$ denotes the z-component of the electric field at the interface between regions ℓ and $\ell-1$ (the interface is approached from the ℓ^{th} region) and χ_0^+ denotes the z-component of the electric field at the interface between regions 1 and 0 (the interface is approached from the 0^{th} region). Expressing (19) in terms of (20) yields

$$\psi_\ell^\pm = \pm w_\ell \chi_\ell^\pm, \tag{21}$$

where

$$w_\ell = -\frac{k_{x,\ell}}{\mu_\ell \omega}. \tag{22}$$

Finally, substituting (18) and (19) into (2b), and using (20) and (21) to simplify the result, yields

$$\begin{aligned} \chi_{\ell+1}^+ + \chi_{\ell+1}^- &= \mathrm{e}^{-\mathrm{i}k_{x,\ell}h_\ell}\chi_\ell^+ + \mathrm{e}^{+\mathrm{i}k_{x,\ell}h_\ell}\chi_\ell^-, \\ w_{\ell+1}\chi_{\ell+1}^+ - w_{\ell+1}\chi_{\ell+1}^- &= w_\ell \mathrm{e}^{-\mathrm{i}k_{x,\ell}h_\ell}\chi_\ell^+ - w_\ell \mathrm{e}^{+\mathrm{i}k_{x,\ell}h_\ell}\chi_\ell^-, \end{aligned} \tag{23}$$

for $\ell = 0,\ldots,p-1$. Notice that (23) has the same form as (17), but the definitions of $\chi_\ell^\pm$ and w_ℓ are different. It can be easily shown that the two linear systems, (17) and (23), are identical if $k_{y,p} = 0$ (*normal* incidence).

4. Linear system

To solve the linear system given by (17) or (23), we rewrite it as

$$\chi_1^\pm = \frac{w_1 \pm w_0}{2w_1}\chi_0^+, \tag{24a}$$

$$\begin{bmatrix}\chi_{\ell+1}^+ \\ \chi_{\ell+1}^-\end{bmatrix} = M_\ell \begin{bmatrix}\chi_\ell^+ \\ \chi_\ell^-\end{bmatrix}, \qquad \ell = 1,\ldots,p-1, \tag{24b}$$

where

$$M_\ell = \frac{1}{2w_{\ell+1}}\begin{bmatrix}(w_{\ell+1}+w_\ell)\,\mathrm{e}^{-\mathrm{i}k_{x,\ell}h_\ell} & (w_{\ell+1}-w_\ell)\,\mathrm{e}^{+\mathrm{i}k_{x,\ell}h_\ell} \\ (w_{\ell+1}-w_\ell)\,\mathrm{e}^{-\mathrm{i}k_{x,\ell}h_\ell} & (w_{\ell+1}+w_\ell)\,\mathrm{e}^{+\mathrm{i}k_{x,\ell}h_\ell}\end{bmatrix}, \tag{25}$$

[7] The symbol is purposely chosen to correspond with that in Section 3.3.1.

for $\ell = 1, \ldots, p-1$. We see that once χ_0^+ is known, $\chi_\ell^\pm$, $\ell = 1, \ldots, p$, can be computed from (24). To compute χ_0^+, we iterate (24b) until $l = p-1$ and then use (24a) to write $\chi_1^\pm$ in terms of χ_0^+ to obtain

$$\begin{bmatrix} \chi_p^+/\chi_0^+ \\ \chi_p^-/\chi_0^+ \end{bmatrix} = \frac{M}{2w_1} \begin{bmatrix} w_1 + w_0 \\ w_1 - w_0 \end{bmatrix}, \tag{26}$$

where

$$M = M_{p-1} M_{p-2} \cdots M_1. \tag{27}$$

From (26) we obtain

$$\frac{\chi_0^+}{\chi_p^+} = \frac{2w_1}{(w_1 + w_0)\, m_{11} + (w_1 - w_0)\, m_{12}}, \tag{28a}$$

$$\frac{\chi_p^-}{\chi_p^+} = \frac{(w_1 + w_0)\, m_{21} + (w_1 - w_0)\, m_{22}}{(w_1 + w_0)\, m_{11} + (w_1 - w_0)\, m_{12}}, \tag{28b}$$

where $\{m_{11}, m_{12}, m_{21}, m_{22}\}$ are the elements of M in (27). Substituting (28a) into (24) yields

$$\frac{\chi_1^\pm}{\chi_p^+} = \frac{w_1 \pm w_0}{(w_1 + w_0)\, m_{11} + (w_1 - w_0)\, m_{12}}, \tag{28c}$$

$$\begin{bmatrix} \chi_{\ell+1}^+/\chi_p^+ \\ \chi_{\ell+1}^-/\chi_p^+ \end{bmatrix} = M_\ell \begin{bmatrix} \chi_\ell^+/\chi_p^+ \\ \chi_\ell^-/\chi_p^+ \end{bmatrix}, \quad \ell = 1, \ldots, p-2. \tag{28d}$$

Notice that the solution to both (17) and (23) is given by (28). However, $\chi_\ell^\pm$ and w_ℓ are given by (14), (16) for the (17) linear system, and by (20), (22) for the (23) linear system. We may always check the *numerical* accuracy of our computational scheme by letting $\ell = p-1$ in (28d) and comparing the *computed* χ_p^+/χ_p^+ ratio to 1.

5. Fundamental invariant in multilayers

In this section, we will derive the *fundamental invariant in multilayers* (FIM) [29, 30] in terms of $\chi_\ell^\pm$ for both the parallel and perpendicular polarization states. Regardless of the polarization state, from (24) we have

$$\left(\chi_{\ell+1}^+\right)^2 - \left(\chi_{\ell+1}^-\right)^2 = \frac{w_\ell}{w_{\ell+1}} \left[\left(\mathrm{e}^{-\mathrm{i}k_{x,\ell} h_\ell} \chi_\ell^+ \right)^2 - \left(\mathrm{e}^{+\mathrm{i}k_{x,\ell} h_\ell} \chi_\ell^- \right)^2 \right], \tag{29a}$$

for $\ell = 0, \ldots, p-1$. In the case of the *parallel* polarization state, substituting (16) into (29) yields

$$\begin{aligned} \frac{\epsilon_{\ell+1}}{k_{x,\ell+1}} \left[\left(\chi_{\ell+1}^+\right)^2 - \left(\chi_{\ell+1}^-\right)^2 \right] \\ = \frac{\epsilon_\ell}{k_{x,\ell}} \left[\left(\mathrm{e}^{-\mathrm{i}k_{x,\ell} h_\ell} \chi_\ell^+ \right)^2 - \left(\mathrm{e}^{+\mathrm{i}k_{x,\ell} h_\ell} \chi_\ell^- \right)^2 \right], \end{aligned} \tag{29b}$$

for $\ell = 0, \ldots, p-1$. In the case of the *perpendicular* polarization state, substituting (22) into (29) yields

$$\begin{aligned} \frac{k_{x,\ell+1}}{\mu_{\ell+1}} \left[\left(\chi_{\ell+1}^+\right)^2 - \left(\chi_{\ell+1}^-\right)^2 \right] \\ = \frac{k_{x,\ell}}{\mu_\ell} \left[\left(\mathrm{e}^{-\mathrm{i}k_{x,\ell} h_\ell} \chi_\ell^+ \right)^2 - \left(\mathrm{e}^{+\mathrm{i}k_{x,\ell} h_\ell} \chi_\ell^- \right)^2 \right], \end{aligned} \tag{29c}$$

for $\ell = 0, \ldots, p-1$. The FIM is given by (29b) and (29c) for parallel and perpendicular polarization states, respectively.

The *physical* significance of the FIM is not clear. It is similar in structure to the $\mathrm{d}s^2$ of special relativity, and under special circumstances reduces to an energy conservation statement. [29, 30] We will discuss the possible generalizations and physical meaning of the FIM in future publications; presently, we use it only as a numerical test.

6. Harmonic electric and magnetic energy density

In the case of a right-handed material (see Section 2.1 for the definition), the time-averaged complex Poynting theorem for harmonic fields is given by

$$\nabla \cdot \mathbf{S} + \frac{1}{2} \mathbf{J}^* \cdot \mathbf{E} + 2\mathrm{i}\omega \left(\hat{u}^{(\mathrm{e})} - \hat{u}^{(\mathrm{m})} \right) = 0, \tag{30}$$

where $\mathbf{S} = \frac{1}{2} \mathbf{E} \times \mathbf{H}^*$ is the complex Poynting vector, $\hat{u}^{(\mathrm{e})} = \frac{1}{4} \mathbf{E} \cdot \mathbf{D}^*$ is the *complex* electric energy density, $\hat{u}^{(\mathrm{m})} = \frac{1}{4} \mathbf{B} \cdot \mathbf{H}^*$ is the *complex* magnetic energy density, and $\mathbf{J}$ is the *impressed* (as opposed to the *conduction*) current density. If $\mathbf{J} = 0$, then (30) yields

$$\nabla \cdot \mathbf{S} + Q^{(\mathrm{e})} + Q^{(\mathrm{m})} + 2\mathrm{i}\omega \left(u^{(\mathrm{e})} - u^{(\mathrm{m})} \right) = 0, \tag{31a}$$

where

$$u^{(\mathrm{e})} = \frac{\epsilon'}{4} \mathbf{E} \cdot \mathbf{E}^* = \frac{\epsilon'}{4} \|\mathbf{E}\|^2, \tag{31b}$$

$$u^{(\mathrm{m})} = \frac{\mu'}{4} \mathbf{H} \cdot \mathbf{H}^* = \frac{\mu'}{4} \|\mathbf{H}\|^2, \tag{31c}$$

$$Q^{(\mathrm{e})} = \frac{\omega \epsilon''}{2} \mathbf{E} \cdot \mathbf{E}^* = \frac{\omega \epsilon''}{2} \|\mathbf{E}\|^2, \tag{31d}$$

$$Q^{(\mathrm{m})} = \frac{\omega \mu''}{2} \mathbf{H} \cdot \mathbf{H}^* = \frac{\omega \mu''}{2} \|\mathbf{H}\|^2. \tag{31e}$$

In (31), $u^{(\mathrm{e})}$ is the *real* time-averaged electric density, $u^{(\mathrm{m})}$ is the *real* time-averaged magnetic density, $Q^{(\mathrm{e})}$ and $Q^{(\mathrm{m})}$ represent time-averaged electric and magnetic losses, respectively (e.g., Joule's heating [31, Sec. 2.19, Sec. 2.20]). Substituting the total electric field and the total magnetic intensity into (31b) and (31c), respectively, yields

$$u_\ell^{(\mathrm{e})} = \frac{\epsilon_\ell'}{4} \left(\left\| \mathbf{E}_\ell^+ \right\|^2 + \left\| \mathbf{E}_\ell^- \right\|^2 + 2\mathrm{Re} \left[\mathbf{E}_\ell^+ \cdot \mathbf{E}_\ell^{-*} \right] \right), \tag{32a}$$

$$u_\ell^{(\mathrm{m})} = \frac{\mu_\ell'}{4} \left(\left\| \mathbf{H}_\ell^+ \right\|^2 + \left\| \mathbf{H}_\ell^- \right\|^2 + 2\mathrm{Re} \left[\mathbf{H}_\ell^+ \cdot \mathbf{H}_\ell^{-*} \right] \right), \tag{32b}$$

where Re denotes the real part.

In the case of the LHM, the complex Poynting theorem for harmonic fields given by (30) and (31) is *mathematically* correct. However, the identification of the real electric density

(31b) and the real magnetic density (31c) is troublesome because both are *negative*. It was pointed out by Veselago [9] that the LHM must be accompanied by frequency dispersion, in which case the real electric density and the real magnetic density are not given by (31b) and (31c), respectively. Moreover, simultaneously negative permittivity and permeability occur very near resonance and therefore for the LHM, there is no frequency interval where permittivity and permeability may be reasonably approximated by a constant. For a more detailed discussion see [12], [32], and [33].

6.1. Energy densities for parallel polarization

It is convenient to introduce a new symbol for the transverse component (the y-component) of the electric field as a function of distance, x, into the multilayer stack. Let

$$\Gamma_\ell^\pm(x) = \pm k_{x,\ell} E_\ell^\pm \exp\left[\pm \mathrm{i} k_{x,\ell} x\right] \tag{33}$$

then,

$$\begin{aligned} \left|\Gamma_\ell^\pm(x)\right|^2 &= \left|k_{x,\ell}\right|^2 \left|E_\ell^\pm\right|^2 \exp\left(\mp 2\mathrm{Im}[k_{x,\ell}]x\right), \\ \mathrm{Re}\left[\Gamma_\ell^+(x)\Gamma_\ell^{-*}(x)\right] &= -\left|k_{x,\ell}\right|^2 \mathrm{Re}\left[E_\ell^+ E_\ell^{-*} \mathrm{e}^{+2\mathrm{iRe}[k_{x,\ell}]x}\right]. \end{aligned} \tag{34}$$

Substituting (13) into (32a) and using (34) to simplify the result yields

$$\begin{aligned} u_\ell^{(\mathrm{e})}(x) =& \frac{\epsilon_\ell'}{4}\left[\left(1 + \frac{k_{y,p}^2}{\left|k_{x,\ell}\right|^2}\right)\left(\left|\Gamma_\ell^+(x)\right|^2 + \left|\Gamma_\ell^-(x)\right|^2\right)\right. \\ &\left. +2\left(1 - \frac{k_{y,p}^2}{\left|k_{x,\ell}\right|^2}\right)\mathrm{Re}\left[\Gamma_\ell^+(x)\Gamma_\ell^{-*}(x)\right]\right]. \end{aligned} \tag{35}$$

Substituting (12) into (32b) and using (34) to simplify the result yields

$$\begin{aligned} u_\ell^{(\mathrm{m})}(x) =& \frac{\mu_\ell' \left|w_\ell\right|^2}{4} \\ &\times \left(\left|\Gamma_\ell^+(x)\right|^2 + \left|\Gamma_\ell^-(x)\right|^2 - 2\mathrm{Re}\left[\Gamma_\ell^+(x)\Gamma_\ell^{-*}(x)\right]\right), \end{aligned} \tag{36}$$

where w_ℓ is given by (16).

6.2. Energy densities for perpendicular polarization

Again, it's convenient to introduce a new symbol for the transverse component (the z-component) of the electric field as a function of distance, x, into the multilayer stack. Let

$$\Gamma_\ell^\pm(x) = E_\ell^\pm \mathrm{e}^{+\mathrm{i} k_{x,\ell} x} \tag{37}$$

then,

$$\begin{aligned} \left|\Gamma_\ell^\pm(x)\right|^2 &= \left|E_\ell^\pm\right|^2 \exp\left(\mp 2\mathrm{Im}[k_{x,\ell}]x\right) \\ \mathrm{Re}\left[\Gamma_\ell^+(x)\Gamma_\ell^{-*}(x)\right] &= \mathrm{Re}\left[E_\ell^+ E_\ell^{-*} \mathrm{e}^{+2\mathrm{iRe}[k_{x,\ell}]x}\right]. \end{aligned} \tag{38}$$

Substituting (18) into (32a) and using (38) to simplify the result yields

$$u_\ell^{(\mathrm{e})}(x) = \frac{\epsilon_\ell'}{4}\left[\left|\Gamma_\ell^+(x)\right|^2 + \left|\Gamma_\ell^-(x)\right|^2 + 2\mathrm{Re}\left[\Gamma_\ell^+(x)\Gamma_\ell^{-*}(x)\right]\right]. \tag{39}$$

Substituting (19) into (32b) and using (38) to simplify the result yields

$$\begin{aligned} u_\ell^{(\mathrm{m})}(x) =& \frac{\mu_\ell' \left|w_\ell\right|^2}{4}\left[\left(1 + \frac{k_{y,p}^2}{\left|k_{x,\ell}\right|^2}\right)\left(\left|\Gamma_\ell^+(x)\right|^2 + \left|\Gamma_\ell^-(x)\right|^2\right)\right. \\ &\left. -2\left(1 - \frac{k_{y,p}^2}{\left|k_{x,\ell}\right|^2}\right)\mathrm{Re}\left[\Gamma_\ell^+(x)\Gamma_\ell^{-*}(x)\right]\right]. \end{aligned} \tag{40}$$

where w_ℓ is given by (22).

7. Transmission and reflection coefficients

The transmission coefficient, T, and the reflection coefficient, R, are given by

$$T = \frac{\mathrm{Re}\left[\mathbf{S}_0^+\right] \cdot \hat{\mathbf{x}}}{\mathrm{Re}\left[\mathbf{S}_p^+\right] \cdot \hat{\mathbf{x}}}, \tag{41a}$$

$$R = -\frac{\mathrm{Re}\left[\mathbf{S}_p^-\right] \cdot \hat{\mathbf{x}}}{\mathrm{Re}\left[\mathbf{S}_p^+\right] \cdot \hat{\mathbf{x}}}, \tag{41b}$$

with

$$\mathbf{S}_0^+ = \frac{1}{2}\mathbf{E}_0^+ \times \mathbf{H}_0^{+*} \qquad \text{and} \qquad \mathbf{S}_p^\pm = \frac{1}{2}\mathbf{E}_p^\pm \times \mathbf{H}_p^{\pm *},$$

where it is understood that $\mathbf{E}_p^\pm$ and $\mathbf{H}_p^{\pm *}$ are evaluated at the interface between regions p and $p-1$ (the interface is approached from the p^{th} region), and $\mathbf{E}_0^+$ and $\mathbf{H}_0^{+*}$ are evaluated at the interface between regions 1 and 0 (the interface is approached from the 0^{th} region).

In the case of the parallel polarization state, substituting (12) and (13) into (41), and using (14) to simplify the result, yields

$$T = \frac{k_{x,p}}{\epsilon_p}\frac{\mathrm{Re}\left[\epsilon_0^* k_{x,0}\right]}{\left|k_{x,0}\right|^2}\left|\frac{\chi_0^+}{\chi_p^+}\right|^2, \tag{42a}$$

$$R = \left|\frac{\chi_p^-}{\chi_p^+}\right|^2. \tag{42b}$$

In the case of the perpendicular polarization state, substituting (19) and (18) into (41), and using (20) to simplify the result, yields

$$T = \frac{\mu_p}{k_{x,p}}\mathrm{Re}\left[\frac{k_{x,0}^*}{\mu_0^*}\right]\left|\frac{\chi_0^+}{\chi_p^+}\right|^2, \tag{43a}$$

$$R = \left|\frac{\chi_p^-}{\chi_p^+}\right|^2. \tag{43b}$$

The transmission and reflection coefficients, given by (42) for the parallel polarization state and by (43) for the perpendicular polarization state, are valid for both a right- and a left-handed material.

8. Numerical computation

Python is a multi-paradigm programming language that supports object-oriented programming, structured programming, and a subset of functional and aspect-oriented programming styles. There is a large number of numerical libraries available for use with Python. Most of these numerical libraries are implemented in middle-level languages such as C, C++ and Fortran. There is some concern about the speed of computations in Python because it is *byte-compiled*, not a compiled language such as Fortran. However, in our opinion, the code readability and ease-of-use of Python (leading to faster development times) in many cases outweigh any performance benefits of middle-level languages. Typically, computationally intensive routines in Python are implemented in middle-level languages and therefore, the difference in computation time between Python and middle-level languages is acceptable for many applications.

Numerical computations associated with the multilayer stack are implemented in an object-oriented programming style with some reliance on a SciPy library.[8] In our opinion, a reader familiar with MATLAB$^{\text{TM}}$ and/or Fortran 90/95 will find SciPy a very natural and easy-to-use library. However, our code can be easily modified to remove the SciPy library dependence in favor of another numerical library such as the GNU Scientific Library (GSL).[9]

9. Multilayer classes

In order for our multilayer classes, namely `Boundary` and `Layer`, to be as useful as possible to the scientific community, we paid particular attention to the readability, usability, and maintainability of the code. In principle, as it was shown in Sections 2–7, in order to compute almost any quantity of interest we need to know the thickness of each layer, permittivity and permeability of each region, and the angle of incidence, state of polarization and frequency of the incident monochromatic plane wave, as well as the transverse component of the electric field evaluated on the interface, i.e., $\chi_\ell^\pm$. However, we found that this set is not the most convenient one to use and therefore we chose a different "minimal" set, described in Table 1. The `Boundary` class is meant to be a base class (*superclass* in the Python lexicon) that will be inherited by the derived classes (*subclasses* in the Python lexicon). The derived classes perform "high-level" computations such as computing the energy density, and the transmission and reflection coefficients. For the `Boundary` class to be an effective base class it must be implemented with performance in mind. It is relatively obvious that the computationally intensive part of the `Boundary` class is the computation of $\chi_\ell^\pm$, i.e., the solution of the linear system described in Section 4. Therefore, the computation of $\chi_\ell^\pm$ is implemented in Fortran 90 and the Python bindings are built by F2PY[10]. It's a common practice within the Python community to implement "workhorse functions" in a middle-level language, however, such practice reduces readability and maintainability to some extent. Therefore, we strongly encourage developers to only implement workhorse functions that lead to severe bottlenecks in middle-level language. It's often the case that the bottlenecks can only be identified after code profiling (performance analysis). For example, it's not obvious that the square root function in the computation of $k_{x,\ell}$, see (8), is relatively time-consuming. The reason computation of $k_{x,\ell}$ is relatively expensive because SciPy's square root function of a complex number $z = |z|e^{i\theta}$ returns $\sqrt{|z|}e^{i\theta/2}$, where $-\pi < \theta \leq \pi$, but (8) requires that $\mathrm{Im}[k_{x,\ell}] > 0$. Moreover, in the case of a perfect dielectric made of a left-handed material, the square root function in (8) must return $k_{x,\ell} = -|k_{x,\ell}|$ (if the second computation scheme is chosen in Section 3.2). Thus, one must convert the square root returned by SciPy to an appropriate quadrant as required by (8), leading to an increase in the computation time of the square root.

The derived `Layer` class inherits the `Boundary` and computes the quantities described in Table 2. The benefit of using inheritance in our multilayer calculations is that other developers may extend the `Layer` class or write their own derived class to compute the desired quantity of interest without having to implement the low-level transfer matrix code.

10. Numerical tests

All numerical computations are performed in double precision; however, the numerical equalities of the de Hoop reciprocity theorem [34, Section 6], complex Poynting theorem (31a) and the fundamental invariant in multilayers, see Section 5, are only tested to single precision. The quantities a and b are considered to be numerically equal (single precision equality, if you will) if $|a - b| \leq 10^{-7}|b|$ and $|b - a| \leq 10^{-7}|a|$

[8] SciPy is free and open-source software available for download from `http://www.scipy.org/`.

[9] Python interface for the GSL is provided by PyGSL and is available from `http://pygsl.sourceforge.net/`.

[10] F2PY (Fortran to Python Interface Generator) is a command line tool for connecting Python with external subroutines written in Fortran 77/90/95 or functions written in C. F2PY is open-source software and may be downloaded from `http://cens.ioc.ee/projects/f2py2e/`.

Table 1: The first column contains the name (as it appears in the code) of the object attribute of the class `Boundary`, the second column contains a description of the attribute, and the third column contains references to a section and/or an equation where a more detailed description of the attribute may be found.

Name	Description	Refs.
`self.h`	thickness of each layer, h_ℓ	(14), (20)
`self.epsRel`	relative permittivity of each region, $\epsilon_\ell/\epsilon_{\text{vacuum}}$	Section 3
`self.muRel`	relative permeability of each region, $\mu_\ell/\mu_{\text{vacuum}}$	Section 3
`self.pol`	polarization state	Section 3.3
`self.kx`	x-component of the wavevector, $k_{x,\ell}$	(8)
`self.w`	scaled `self.kx` (polarization dependent), w_ℓ	(16), (22)
`self.chiPlus`	transverse component of the electric field evaluated on the interface, χ_ℓ^+/χ_p^+	(14), (20)
`self.chiMinus`	transverse component of the electric field evaluated on the interface, χ_ℓ^-/χ_p^+	(14), (20)

Table 2: The first column contains the name (as it appears in the code) of the object attribute (method) of the class `Layer`, the second column contains a description of the method, and the third column contains references to the section where a more detailed description may be found.

Name	Description	Refs.
`field`	transverse component of the electric field as a function of distance, $\Gamma^{\pm}(x)$	6.1, 6.2
`energy`	electric/magnetic energy density as a function of distance, $u^{(\text{e,m})}(x)$	6.1, 6.2
`loss`	electric/magnetic losses as a function of distance, $Q^{(\text{e,m})}(x)$	6
`divPoynting`	divergence of the Poynting vector as a function of distance, $\nabla \cdot \mathbf{S}(x)$	6
`FIM`	FIM at each boundary interface	5
`FIMvsDist`	FIM as a function of distance	5

`TRvsFreq`
`TRvsAngle`
`TRvsFreqAndAngle`
	transmission and reflection coefficients as a function of frequency $f = \omega/2\pi$ and/or angle of incidence ϕ, i.e., $\{T(f), R(f)\}$, $\{T(\phi), R(\phi)\}$, $\{T(f,\phi), R(f,\phi)\}$	7

or $|a - b| \leq 10^{-38}$. Our definition of numerical equality may appear to be too loose, but that is not the case if one considers a scenario when $\text{Im}\,[k_{x,\ell}h_\ell]$ is large. In this scenario, the left-hand side of the transfer matrix M_ℓ, given by (25), grows exponentially and the right-hand side of M_ℓ decreases exponentially, which leads to "numerical swamping." By numerical swamping, we mean the mixing of extremely large terms with extremely small terms, where extremely large/small terms are understood in the double precision sense. Numerical swamping may lead to underflow/overflow errors, as well as a loss of accuracy because the extremely small terms effectively become zero. Roughly speaking, single precision equality is maintained if $0 \lesssim \text{Im}\,[k_{x,\ell}h_\ell] \lesssim 3$ and the maximum number of layers is on the order of a hundred.

We have also verified that our code satisfies Weston's theorem [35]. For the reader's convenience, we state Weston's theorem here without proof.

Theorem 1. *If a plane electromagnetic wave is incident upon a body composed of material such that $\epsilon_{relative} = \mu_{relative}$, then the far zone back-scattered field is zero, provided that the direction of incident propagation is parallel to an axis of the body about which a rotation of 90° leaves the shape of the body together with its material medium invariant.*

In our case of a planar stratified media, Weston's theorem simply states that $\chi_\ell^- = 0$ for a normally incident monochromatic plane wave. This result may be immediately derived from Section 4 by noting that $w_0 = w_{\ell=1,\ldots,p}$ and consequently, the transfer matrix M_ℓ reduces to

$$M_\ell = \begin{bmatrix} \mathrm{e}^{-\mathrm{i}k_{x,\ell}h_\ell} & 0 \\ 0 & \mathrm{e}^{+\mathrm{i}k_{x,\ell}h_\ell} \end{bmatrix}, \qquad \ell = 1, \ldots, p-1. \tag{44}$$

However, because of subtractive cancellation [36], $w_{\ell+1} - w_\ell = \delta_\ell$, where δ_ℓ is small but usually non-zero for $\ell = 0, \ldots, p-1$. Therefore, the off-diagonal elements of (44) are generally non-zero and because of the iterative nature of the transfer matrix algorithm, these "small" elements may contribute significantly to χ_ℓ^-. In other words, χ_ℓ^- should *not* be compared to zero even in a single precision sense, e.g., in some circumstances we have observed χ_ℓ^- to be as large as 10^{-15}. In light of the above discussion, we choose to test single precision numerical equality of $\chi_\ell^+ + \chi_\ell^-$ to χ_ℓ^+ because χ_ℓ^+ tends to be many orders of mag-

nitude larger than χ_ℓ^-. With this definition of equality, our code satisfies Weston's theorem.

11. Conclusions

A transfer matrix algorithm for electromagnetic wave propagation through planar stratified media composed of a right-handed and/or left-handed material has been implemented in Python. Pathological cases caused by unphysical approximation of zero absorption have been carefully examined and numerically circumvented (see Section 3.2). The numerical computations were implemented in an object-oriented programming style by dividing them into two classes, `Boundary` and `Layer`. The `Boundary` class performs computationally intensive calculations, namely the solution of the linear system described in Section 4 and the square root of $k_{x,\ell}^2$. The workhorse functions of the `Boundary` class were implemented in Fortran 90 in order to avoid computational bottlenecks. The `Layer` class performs high-level calculations such as calculation of $u^{(\mathrm{e,m})}(x)$, $Q^{(\mathrm{e,m})}(x)$, $\Gamma^{\pm}(x)$ and FIM. The code has been thoroughly tested and, roughly speaking, can be trusted to single precision if $0 \lesssim \mathrm{Im}\,[k_{x,\ell} h_\ell] \lesssim 3$ and the maximum number of layers is on the order of a hundred (see Section 10).

We hope that our open-source and object-oriented implementation of the transfer matrix algorithm, which is suitable for modern applications such as Anderson localization of light and perfect lensing, will be adapted by a wide scientific community. At the very least, we hope that our publicly available implementation of the transfer matrix algorithm will encourage the scientific community to use open-source software, thus enhances the reproducibility of scientific work.

[1] J. M. Vigoureux, Polynomial formulation of reflection and transmission by stratified planar structures, J. Opt. Soc. Am. A 8 (1991) 1697–1701.
[2] T. El-Agez, S. Taya, A. El Tayyan, A polynomial approach for reflection, transmission, and ellipsometric parameters by isotropic stratified media, Optica Applicata 40 (2010) 501–510.
[3] J. M. Vigoureux, Use of Einstein's addition law in studies of reflection by stratified planar structures, J. Opt. Soc. Am. A 9 (1992) 1313–1319.
[4] J. J. Monzón, L. L. Sánchez-Soto, Fully relativisticlike formulation of multilayer optics, J. Opt. Soc. Am. A 16 (1999) 2013–2018.
[5] R. L. Mooney, An exact theoretical treatment of reflection-reducing optical coatings, J. Opt. Soc. Am. 35 (1945) 574–574.
[6] W. Weinstein, The reflectivity and transmissivity of multiple thin coatings, J. Opt. Soc. Am. 37 (1947) 576–577.
[7] F. Abelès, La théorie générale des couches minces, J. Phys. Radium 11 (1950) 307–310.
[8] M. Born, E. Wolf, Principles of Optics: Electromagnetic Theory of Propagation, Interference and Diffraction of Light, Pergamon Press, Oxford, sixth (corrected) edition, 1986.
[9] V. G. Veselago, The electrodynamics of substances with simultaneously negative values of ϵ and μ, Soviet Physics Uspekhi 10 (1968) 509–514.
[10] D. R. Smith, W. J. Padilla, D. C. Vier, S. C. Nemat-Nasser, S. Schultz, Composite medium with simultaneously negative permeability and permittivity, Phys. Rev. Lett. 84 (2000) 4184–4187.
[11] R. A. Shelby, D. R. Smith, S. Schultz, Experimental verification of a negative index of refraction, Science 292 (2001) 77–79.
[12] S. A. Ramakrishna, Physics of negative refractive index materials, Reports on Progress in Physics 68 (2005) 449–521.
[13] J. B. Pendry, Negative refraction makes a perfect lens, Phys. Rev. Lett. 85 (2000) 3966–3969.
[14] M. Scalora, G. D'Aguanno, N. Mattiucci, M. J. Bloemer, D. de Ceglia, M. Centini, A. Mandatori, C. Sibilia, N. Akozbek, M. G. Cappeddu, M. Fowler, J. W. Haus, Negative refraction and sub-wavelength focusing in the visible range using transparent metallo-dielectric stacks, Opt. Express 15 (2007) 508–523.
[15] E. Abrahams (Ed.), 50 Years of Anderson Localization, World Scientific, New Jersey, 2010.
[16] P. Sheng, Introduction to Wave Scattering, Localization and Mesoscopic Phenomena, Springer, Berlin, second edition, 2006.
[17] J. A. Scales, L. D. Carr, D. B. McIntosh, V. Freilikher, Y. P. Bliokh, Millimeter wave localization: Slow light and enhanced absorption in random dielectric media, Phys. Rev. B 76 (2007) 085118.
[18] K. Y. Bliokh, V. D. Freilikher, Localization of transverse waves in randomly layered media at oblique incidence, Phys. Rev. B 70 (2004) 245121.
[19] A. A. Asatryan, S. A. Gredeskul, L. C. Botten, M. A. Byrne, V. D. Freilikher, I. V. Shadrivov, R. C. McPhedran, Y. S. Kivshar, Anderson localization of classical waves in weakly scattering metamaterials, Phys. Rev. B 81 (2010) 075124.
[20] R. Giust, J. M. Vigoureux, M. Sarrazin, Asymmetrical properties of the optical reflection response of the Fabry–Pérot interferometer, J. Opt. Soc. Am. A 17 (2000) 142–148.
[21] S. V. Zhukovsky, Perfect transmission and highly asymmetric light localization in photonic multilayers, Phys. Rev. A 81 (2010) 053808.
[22] A. Markushevich, Theory of Functions of a Complex Variable, Chelsea Publishing Company, New York, second edition, 1977. 3 volumes in one, translated from Russian by Richard A. Silverman.
[23] E. J. Rothwell, M. J. Cloud, Electromagnetics, CRC Press, Boca Raton, FL, second edition, 2008.
[24] B.-N. Jiang, J. Wu, L. A. Povinelli, The origin of spurious solutions in computational electromagnetics, J. Comput. Phys. 125 (1996) 104–123.
[25] I. D. Mayergoyz, J. D'Angelo, A new point of view on the mathematical structure of Maxwell's equations, Magnetics, IEEE Transactions on 29 (1993) 1315–1320.
[26] L. D. Landau, E. M. Lifshitz, Electrodynamics of Continuous Media: Part 1, volume 5, Pergamon Press, Oxford, third revised and enlarged edition, 1993. Translated from Russian by J. B. Sykes and M. J. Kearsley.
[27] L. D. Landau, E. M. Lifshitz, P. L. Petrovich, Electrodynamics of Continuous Media, volume 8, Pergamon Press, Oxford, second revised and enlarged edition, 1993. Translated from Russian by J. B. Sykes, J. S. Bell and M. J. Kearsley.
[28] J. Skaar, On resolving the refractive index and the wave vector, Optics Letters 31 (2006) 3372–3374.
[29] J. M. Vigoureux, P. Grossel, A relativistic-like presentation of optics in stratified planar media, American Journal of Physics 61 (1993) 707–712.
[30] J. M. Vigoureux, R. Giust, New relations in the most general expressions of the transfer matrix, Optics Communications 186 (2000) 21–25.
[31] J. A. Stratton, Electromagnetic Theory, McGraw-Hill, New York, 1941.
[32] R. Ruppin, Electromagnetic energy density in a dispersive and absorptive material, Physics Letters A 299 (2002) 309–312.
[33] A. M. Vadim, Correct definition of the Poynting vector in electrically and magnetically polarizable medium reveals that negative refraction is impossible, Optics Express 16 (2008) 19152–19168.
[34] R. J. Potton, Reciprocity in optics, Rep. Prog. Phys. 67 (2004) 717–754.
[35] V. H. Weston, Theory of absorbers in scattering, IEEE Trans. Antennas Propag. 11 (1963) 578–584.
[36] D. Goldberg, What every computer scientist should know about floating-point arithmetic, ACM Computing Surveys 23 (1991) 5–48.